Earth Surface Processes and Landforms
Earth Surf. Process. Landforms **25**, 239–253 (2000)

AEOLIAN SAND TRANSPORT AT THE LANPHERE DUNES, NORTHERN CALIFORNIA

MITCHELL S. CRAIG*

Geology Department, University of Papua New Guinea Box 414, University PO, NCD, Papua New Guinea

Received 10 March 1997; Revised 5 April 1999; Accepted July 1999

ABSTRACT

Aeolian sand transport was studied at the Lanphere Dunes, a coastal dune complex in northern California, by comparing slipface advance rates with transport predicted based on local wind data. The slipfaces of a 2·5 m high transverse ridge and 10 m high parabolic dune were monitored over a period of three months to estimate sand discharge. The study was performed during the dry season, which has the maximum sand-driving potential. Over the three month study period, average sand discharge was 12·5 m^3 per m width per year at the transverse ridge and 8·8 m^3 per m width per year at the parabolic dune.

A method was developed for modelling slipfaces that are sinuous and where sediment transport rates are not constant across the width of the slipface. Field measurements were used to generate three-dimensional representations of dune slipfaces. Periodic measurements over the course of three months were used to compute the volume of displaced sediment.

Theoretical sand transport was computed from local wind data using the Bagnold model and compared with the observed transport rates. Predicted rates were substantially lower than observed rates. Wind velocities rarely exceeded the threshold velocity. Discrepancies between the observed and predicted values appear to be caused by a combination of wind data recording procedures and differences between wind velocities at the anemometer location and the site where sand transport was measured.

Wind data collected by weather bureaux have been utilized in numerous studies for modelling sediment transport. Such data typically have sample intervals of one hour or greater and are often averaged prior to reporting. The effect of averaging was investigated by comparing sand transport estimates based on daily average wind velocities with those based on the original hourly observations. The daily average data were depleted of high velocity winds and sand transport estimates were accordingly much lower than those based on the hourly data.

KEY WORDS: wind; sand dunes; sediment transport; aeolian sand transport; California coast; field methods

INTRODUCTION

This study was undertaken to measure sand transport rates at a coastal dunefield and compare them with predictions based on local wind data. Sand transport was measured at the Lanphere Dunes, which are located on the northern California coast approximately 10 km north of Eureka and 160 km south of the Oregon border (Figure 1). These dunes are part of a dune belt several kilometres long which is bounded on the west by a vegetated foredune ridge and the ocean, and on the east by forest (Figures 2 and 3). An overview of the coastal dunes of California was given by Cooper (1967).

Sand transport at the Lanphere Dunes is essentially unidirectional, as marked by the consistent orientations of prominent longitudinal ridges. Transport rates were computed by measuring the positions of slipfaces relative to marker stakes and compared with sand transport predicted using the Bagnold model with wind data from the Eureka Weather Service, located about 10 km to the south.

Aeolian sand transport rates have been measured in previous studies based on both sequential aerial photographs and ground monitoring.

* Correspondence to: Dr M. S. Craig, Geology Department, University of Papua New Guinea, Box 414, University PO, NCD, Papua New Guinea. E-mail: craig@upng.ac.pg

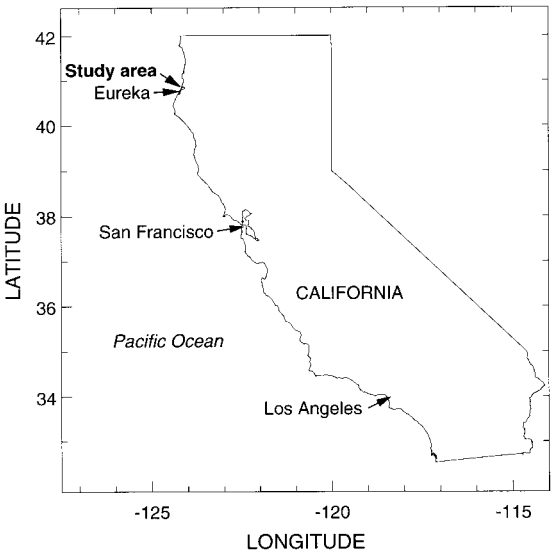

Figure 1. The study area is located approximately 10 km north of Eureka, on the coast of northern California

Aerial photographs have generally been used to compute dune migration rates of large dunes over periods of several decades. Pickard (1972) measured dune movement at Cronulla, Australia, from a series of aerial photographs spanning 35 years. Hunter *et al.* (1983) computed sand transport rates in the Oregon Dunes, USA, from air photos spanning 36 years and compared them with transport rates computed using the Bagnold (1941) model with one year of wind data. Illenberger and Rust (1988) estimated sand transport rates in the Alexandria dunefield in South Africa from air photos spanning 40 years; and compared the observed rates with theoretical transport determined with the Bagnold model from eight months of wind data.

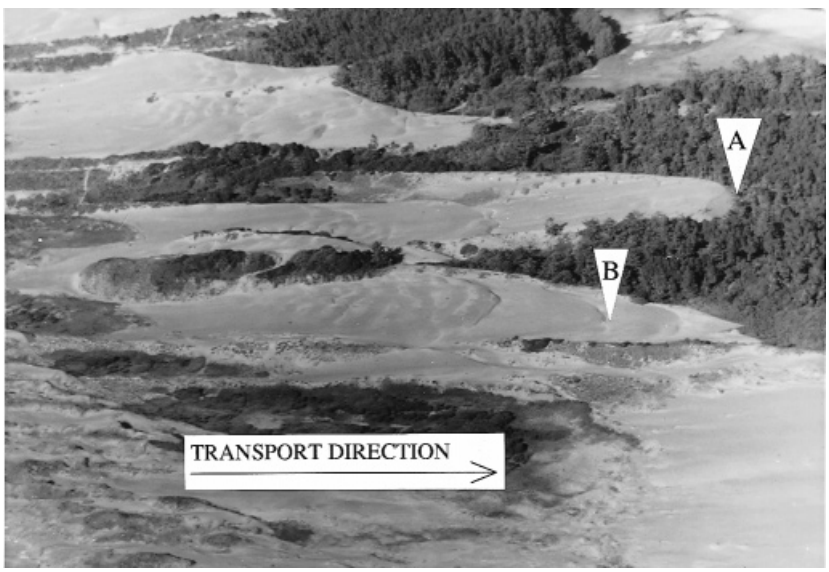

Figure 2. Study area, looking northeast. Arrows point to slipfaces of parabolic dune (A) and transverse ridge (B) monitored in this study. Predominant wind blows from left to right, i.e. from north-northwest to south-southeast (photograph by L. Baker, 1975–76)

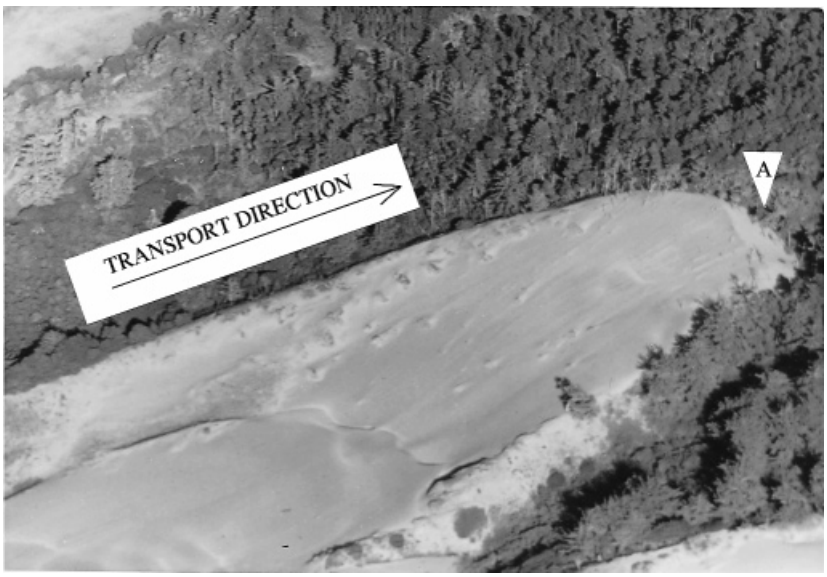

Figure 3. Parabolic dune and slipface, looking east. Arrow A indicates slipface monitored in this study (photograph by L. Barker, 1975–76)

Ground monitoring in previous studies has been based on data collected from sediment traps and repeated measurements of dune features. Bauer *et al.* (1990) deployed sediment traps and vertical arrays of anemometers in a study comparing the Bagnold and Kawamura models with observed sediment transport. Mulligan (1988) measured wind velocity gradients and sediment transport at a coastal dune complex and discussed implications for the accuracy of Bagnold-type models. Livingstone (1989) monitored changes in the cross-profile of a linear dune relative to a network of fixed posts. Sarre (1989) measured changes in the longitudinal profile of a dune and compared them with sand transport computed from concurrent wind data.

Previous estimates of sand transport at the Lanphere Dunes were reported by Johnson (1963a), who monitored dune advance rates in the field by measuring dune crestlines relative to a single fixed stake, and Weaver (1991), who mapped parabolic dune fronts in the field and plotted their locations on large-scale aerial photographs from four years prior.

In the present work, field measurements were used to represent the slipfaces of a transverse ridge and parabolic dune in three-dimensional coordinate space. Repeat measurements were made several times during a three month study period and were used to compute sand transport rates. Hourly wind data collected during the same time period at a site 10 km away were used with the Bagnold model to predict sand transport.

Several models that predict sand transport based on wind data have been proposed since Bagnold's (1941) original work. For a review of some of the most frequently cited models, see Johnson (1963b), Lettau and Lettau (1978), Sarre (1988) and McEwan and Willetts (1994). The Bagnold (1941) model has been the most widely employed, and was used in this study because it was expected to give reasonable results and also to facilitate the comparison of the present work with results from previous studies.

SAND DISPLACEMENT MEASUREMENT

Overview

Sand transport was monitored at slipfaces on two strips of mobile sand (Figure 2) approximately 70 m wide by 500 m long. These strips form sand transport corridors that are bounded laterally by vegetated longitudinal ridges. They are oriented north-northwest (parallel with the principal dry-season wind direction) and

culminate in parabolic slipfaces up to 10 m high, which are currently encroaching on a beach pine forest (Figure 3). Transverse ridges up to 3 m high occur in the middle to upper reaches of the active sand strips.

Dune advance rates were computed by measuring slipface position relative to fixed marker stakes. A 2 m high transverse ridge (B in Figure 2) and a 10 m high parabolic dune (A in Figures 2 and 3) were monitored for three months. At both locations, sand transport was estimated by measuring the advance of a section of slipface approximately 30 m wide, which spanned most of the width of the active transport corridors.

Sand discharge was estimated by calculating the volume of sand added to a slipface between successive field measurements. The spatially varying thickness of a new layer of sand accreted to the slipface was determined from ground measurements and integrated over the area of the slipface, i.e. each new layer was approximated as a series of tabular cells distributed laterally along the slipface, and its volume was determined by summing the individual cell volumes.

Ground monitoring, transverse ridge

A transverse ridge located on one of the main corridors of active transport (approximate location indicated by B in Figure 2) was monitored for a period of three months (June–August 1982). The slipface of the transverse ridge was approximately 2 m high and 40 m wide. The central portion (30 m wide) of the slipface was monitored by measuring its position relative to a grid of 1·5 mm diameter steel welding rods. Grid lines were spaced 3 m apart, oriented parallel to the longitudinal axis of the main sand transport corridor, and perpendicular to the transverse ridge, in order to facilitate measurement of slipface movement in the direction 164° (SSE).

Slipface position was monitored by measuring the distances along each longitudinal grid line between the base of the slipface and the nearest marker stake. Since these distances were typically several centimetres, the 1·5 mm diameter marker rods had negligible impact on the sediment transport process. Slipface height was determined by measuring slipface length and multiplying by the sine of slipface slope, which was consistently observed to be 33°. A three-dimensional model of the transverse ridge constructed from field measurements is shown in Figure 4.

Eight surveys of the position of the slipface base were made during the three month study period. Sand volume displacement was computed for each measurement interval, and the cumulative discharge for the three month period is shown in Figure 5.

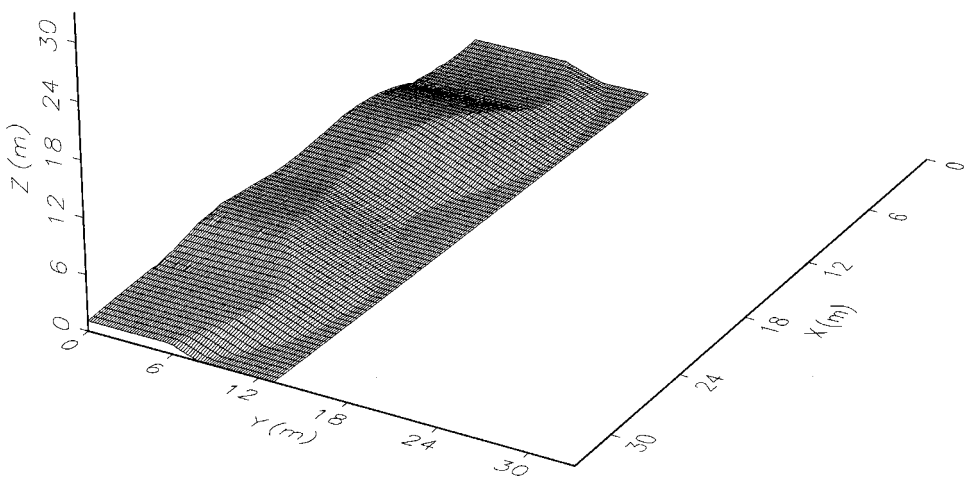

Figure 4. Slipface of transverse ridge. The slipface is progressing in the positive *y* direction, to the south-southeast

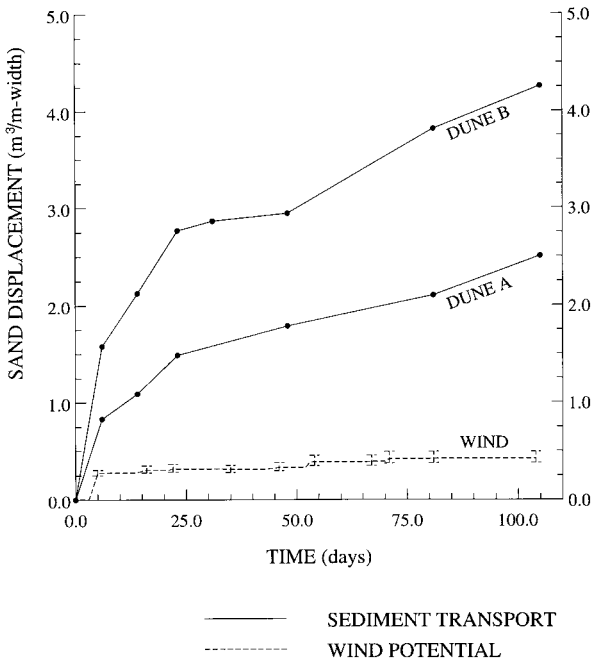

Figure 5. Comparison of predicted (dashed) and observed (solid) sand transport at slipfaces of dune A (parabolic dune) and dune B (transverse ridge)

Ground monitoring, parabolic dune

A 10 m high parabolic slipface was also monitored for the same three month period using a reference grid of marker stakes. This slipface is at the leeward end of an active sand transport corridor (Figures 2 and 3), and is encroaching on a pine forest.

Three measurement lines spanning a 26 m wide section of the parabolic slipface were established using marker stakes at the base of the slipface. The lines were oriented normal to the slipface base. The volume of sand displaced between measurements was computed as described below. Cumulative displacement is shown in Figure 5 with the solid curve labelled 'Dune A'.

Geometry assignment

Figure 6 shows a typical cell used in the volume computations. The lateral sides of each cell are vertical and pass through adjacent longitudinal grid lines. The top and bottom are defined by horizontal planes that intersect the top and base of the slipface. The front and back surfaces coincide with the positions of the slipface at the times of consecutive measurements and are assumed to be planar. The front, back and lateral bounding sides are parallelograms. The top and bottom are trapezoids. The thickness dy (see Figure 6) represents the longitudinal distance between two successive positions of the slipface, and is specified independently for both sides of the cell. The width dx is the spacing between grid lines in the transverse direction. The model was constrained by the following assumptions:

- Temporal changes in dune height during the three month study period were minor compared to the changes in the longitudinal position of the slipfaces and were not considered in the volume computations.
- The slopes of the slipfaces were constant at 33°, measured in the longitudinal direction. This assumption was based on several field measurements and leads to a reasonably simple geometric model, e.g. adjacent cells join smoothly along longitudinal boundaries. In a more rigorous model, slope would be measured in the direction normal to the top edge of the slipface, but since the portion of the slipfaces monitored in this

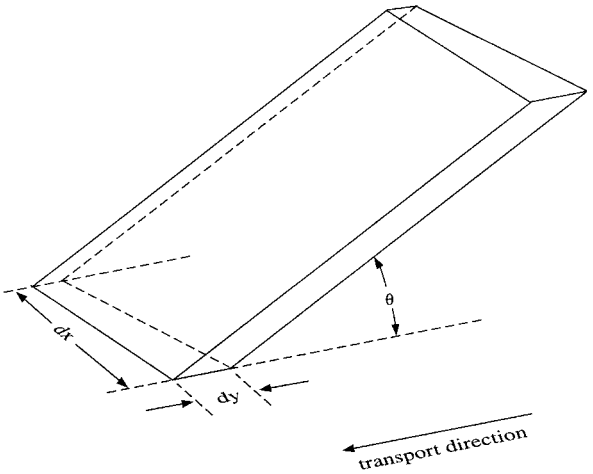

Figure 6. Cell geometry used in sand transport discharge computations. A layer of sand accreted to a slipface is modelled with a series of cells laterally distributed along the slipface

study was of low sinuosity, the difference in volumes computed using the two different methods would be less than 5 per cent.

- The segments of the brink and base that are part of a slipface surface for any given cell are horizontal and parallel. No restrictions are placed on the slope of the back dune area; the model considers only the volume of sand that is added to the slipface during the period of observation.
- It was assumed that most of the sand passing over the brink of a ridge or dune lands on the slipface rather than leaping completely over it, as observed by Anderson (1988) for typical sand sizes and wind conditions. There were no indications of significant amounts of sediment blown clear of the slipface, e.g. a decrease in slope and grainfall deposits near the base of the slipface (Hunter *et al.*, 1983). In situations when wind velocity is high enough such that these conditions are no longer the case, slipface advance rates will provide a lower limit on total sand transport rates.

Volume computation

In order to determine the differential volume of sand corresponding to the slipface advance between successive measurements, individual cell volumes were calculated and summed over the slipface area for each measurement period. Individual cell volumes were computed as

$$V_j = \frac{(\ell_i + \ell_{i+1})}{2} \quad \frac{\mathrm{d}x(\mathrm{d}y_j + \mathrm{d}y_{j+1})}{2} \sin\theta \tag{1}$$

where $\mathrm{d}y_i$ and $\mathrm{d}y_{i+1}$ are longitudinal displacements of the slipface along adjacent grid lines, on either side of a cell; l_i and l_{i+1} are lengths of the two longitudinal faces of the cell, measured in the direction of slipface dip; and θ is the dip of the slipface. The total volume of the layer of sand was obtained by summing the volumes of all the cells along the slipface.

The average discharge at the transverse ridge was 12·5 m^3 per m width per year. The parabolic slipface had an average advance rate of 8·9 m^3 per m width per year over this period, which was consistently about two-thirds of the advance rate measured at the transverse ridge. Apart from the differences in the absolute amount of sand transport, the two dunes responded similarly to winds during the study period.

WIND DATA ANALYSIS

Introduction

One of the principal goals of this work was to compare field observations of sediment transport with theoretical estimates of sand transport based on wind data. This section describes the wind data and how they were used to model sand transport.

Wind data covering the study period were obtained from the National Weather Service in Eureka. The primary data set consists of wind velocities and directions recorded as 1 min averages taken once per hour. Data of this form were used for analysis over a three month period during which sediment transport measurements were made. The Eureka Weather Service is located at the downtown Post Office building, and is 10 km south of the dunes where sand transport was measured. Wind data have been recorded there since 1886 and the present anemometer height of 27 m above ground has been maintained since 1911.

Prediction of sand transport from wind data

The Bagnold aeolian sand transport model was used in this study to predict sand discharge based on wind velocity and sand properties. The key elements of the model are reviewed in the following sections.

Threshold shear velocity. Shear velocity is the fundamental parameter for modelling aeolian sand transport. It is a function of the shear stress exerted by the wind on the sand surface, and provides a measure of the vertical velocity gradient. Shear velocity may be written as:

$$u_* = \sqrt{\frac{\tau}{\rho}} \tag{2}$$

where τ is shear stress and ρ is fluid density. Although u_* has units of velocity it is not directly measured. It may be computed from observations of normal wind velocity (e.g. Bagnold, 1941, pp. 49, 50):

$$u_* = \kappa \frac{v(z_2) - v(z_1)}{\ln(z_2/z_1)} \tag{3}$$

where κ is von Karman's constant, and v is the normal (direct) wind velocity measured at heights z_1 and z_2 (Prandtl, 1934, pp. 133–134).

The minimum shear velocity necessary to entrain sand grains by wind is known as the *fluid threshold* and the minimum shear velocity necessary to sustain entrainment is called the *impact threshold*. Only the latter will be discussed in this work; it was given by Bagnold (1941, pp. 86, 101, 104) as:

$$u_{*t} = A\sqrt{\frac{(\rho_p - \rho_a)gd}{\rho_a}} \tag{4}$$

where $A = 0{\cdot}08$ is the empirical coefficient (for impact threshold); $\rho_p = 2{\cdot}65 \times 10^3$ kg m^{-3} is density of sand particles; $\rho_a = 1{\cdot}22$ kg m^{-3} is density of air; $g = 9{\cdot}81$ m s^{-2} is gravitational acceleration; and $d = 0{\cdot}25$ mm is sand grain diameter at study area.

The values listed above yield an impact threshold of $u_{*t} = 0{\cdot}184$ m s^{-1}. A sand grain diameter of $d = 0{\cdot}25$ mm is consistent with size analyses performed in the study area (Johnson, 1963a) and is a typical value for dune sand.

Threshold normal velocity. Bagnold (1941, pp. 58, 59, 82, 100) showed that wind gradients corresponding to different shear velocities all emanate from a common focus at the top of the saltation zone, commonly referred to as the focal height (Figure 7). The focal height appears to depend on ripple height and is on the

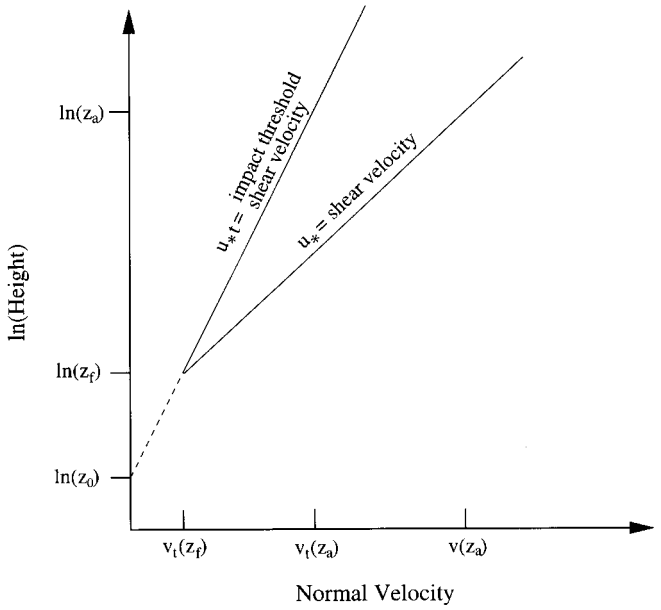

Figure 7. Schematic diagram showing shear velocity profiles. The impact threshold is given by the line labelled u_{*t}, whose slope is u_{*t}/κ, where κ = von Karman's constant. The line labelled u_* has a slope of u_*/κ and corresponds to an arbitrary shear velocity that exceeds the impact threshold

order of 1 cm for normal dune sand (Bagnold, 1941, p. 104). Note that the slopes of the lines labeled u_* and u_{*t} in Figure 7 are u_*/κ and u_{*t}/κ, respectively (shear velocity divided by von Karman's constant).

Using Equation 3 and the threshold shear velocity, we can compute threshold normal velocity at any height above the zero velocity height:

$$v_t(z) = \frac{u_{*t}}{\kappa} \ln\left(\frac{z}{z_0}\right) \qquad \text{if } z > z_0 \tag{5}$$

where v_t is impact threshold normal velocity; $u_{*t} = 18{\cdot}4$ cm s^{-1} is impact threshold shear velocity from Equation 4; $\kappa = 0{\cdot}4$ is von Karman's constant; $z_0 = 8{\cdot}33 \times 10^{-4}$ cm is height of zero velocity, $z_0 = 1/30$ sand grain diameter.

Threshold normal velocities v_t at the presumed focal height of $z_f = 1$ cm and the anemometer height of the Eureka weather station, $z = 26{\cdot}8$ m, were computed (using Equation 5) to be 326 cm s^{-1}, and 689 cm s^{-1}, respectively.

In cases where observed wind velocity exceeds the threshold normal velocity at the observation height (for the Eureka data, $v > 689$ cm s^{-1}), shear velocity may be computed using Equation 3:

$$u_* = \kappa \frac{v(z_a) - v_t(z_f)}{\ln(z_a/z_f)} \tag{6}$$

where $v(z_a)$ is the observed wind velocity at the anemometer height z_a, and $v_t(z_f)$ is the threshold normal velocity at the focal height. Note that $v_t(z_f)$ is written in place of $v(z_f)$ since the two are equal even when wind velocity exceeds the threshold normal velocity at greater heights (see Figure 7). Shear velocity, u_*, will be used in the following section to estimate sand transport.

Theoretical sand displacement. Sand discharge was calculated based on Bagnold's (1941) model:

$$Q = C\sqrt{\frac{d}{D}}\frac{\rho}{g}u_*^3 \tag{7}$$

where $C = 1{\cdot}8$ is an empirical constant, $\rho = 1{\cdot}22 \times 10^{-3}$ gm cm^{-3} density of air, is D is a standard sand grain diameter of 0·25 mm, and d is the size of the sand undergoing transport, also 0·25 mm in this study. We may utilize a discrete series of wind velocity measurements by rewriting Equation 7 as follows:

If $v_i(z_a) > v_t(z_a)$

$$Q = C\sqrt{\frac{d}{D}}\frac{\rho}{g}\left[\frac{\kappa}{\ln(z_a/z_f)}\right]^3\sum_{i=1}^{N}[v_i(z_a) - v_t(z_f)]^3 \tag{8}$$

otherwise

$$Q = 0$$

where $v_i\,(z_a)$ is the wind velocity observed at the anemometer height and $v_t\,(z_f)$ is the threshold velocity at the focal height.

We stipulate above that the predicted sand transport Q shall be set to zero if $v\,(z_a) \leq v_t\,(z_a)$, i.e. the observed velocity fails to exceed the threshold velocity at the instrument height. Equivalently, sand transport occurs only when shear velocity u_* exceeds the threshold value, u_{*t}.

Directionality of sand transport. The direction of sand transport in the study area is controlled primarily by wind distribution but is also influenced by topography. The dune slipfaces monitored in this study were driven by north-northwest winds along well established corridors bounded by vegetated longitudinal ridges. Slip faces were oriented perpendicular to wind direction and spanned most of the width of the transport corridors. The orientation of the longitudinal axes of the main transport corridors is 164°, measured clockwise from north. The corridors were oriented parallel to the principal wind direction.

Sand transport potential in the longitudinal direction during a given time period was computed from the wind data as follows:

$$P = \sum_{i=1}^{N} Q_i\ \cos(\theta_i - \theta_0) \tag{9}$$

where Q_i = sand discharge during ith time interval; θ_i = wind azimuth during time interval i; θ_0 = orientation of transport corridors, 164°, SSE.

THEORETICAL VERSUS OBSERVED SAND TRANSPORT

Sand transport estimates were computed from the Bagnold model for the 103 day study period. The total volume per m width, calculated using the Eureka wind data with Equation 9, was was 0·42 m^3 per m width, far less than the observed displacements, which were 2·5 m^3 per m width for the parabolic dune and 4·3 m^3 per m width for the transverse ridge.

The predicted sand transport using the original wind data is shown as the lowermost dashed curve in Figure 5 and the observed sand transport at dunes A and B is shown by the two solid curves. The precision of transport measurements should be higher at dune B (the transverse ridge) than at dune A (the parabolic dune) owing to the use of a denser measurement grid. The predicted sand transport is much lower than the observed

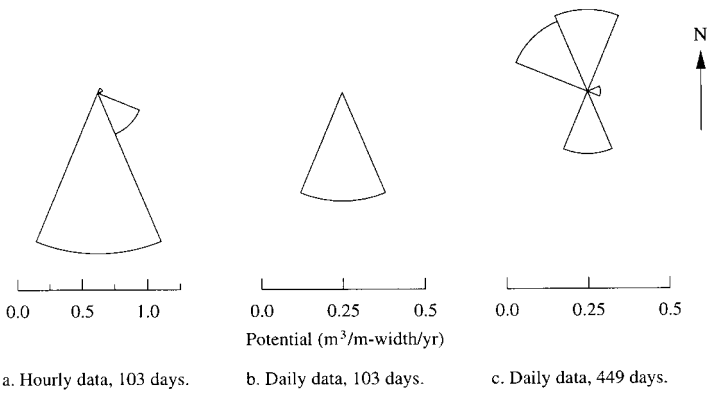

Figure 8. Sand transport potential based on wind data from National Weather Service, downtown Eureka. (a) Hourly data, 103 days; (b) daily averages, 103 days; (c) daily averages, 449 days

transport at either dune. Error bars on the dashed curve indicate the uncertainty in transport predictions associated with the precision of wind velocity measurements. Note that the observed transport steadily increases over time whereas the predicted transport occurs only in a few short episodes. There is a large jump in the predicted values during days 4 and 5, during which over 65 per cent of the predicted transport occurred. Only approximately 25 per cent of the actual transport measured at dune B occurred on these days. It is clear that sand transport is initiated at the dunes well before wind velocity values in the Eureka data reach the threshold velocity specified by the Bagnold model.

AZIMUTHAL VARIATIONS IN SAND TRANSPORT

Sand roses

Sand transport as a function of azimuth was determined by computing a vector contribution for each time sample and summing all contributions in azimuthal bins, i.e. the vector form of Equation 9:

$$\mathbf{P} = \sum_i Q_i \mathbf{e}_i \Delta t \tag{10}$$

where $\mathbf{e}_i$ is a unit vector of wind direction at time sample i.

Azimuthal sand transport potentials were computed using Equation 10 with local wind data and are displayed using sand roses in Figures 8 and 9. The sand transport predicted in a given direction is indicated by the radial length of the sector in that direction.

Hourly wind observations from the three month study period were used to compute the sand roses shown in Figure 8a. Daily averages, which were obtained from the National Weather Service monthly summaries, were used to prepare sand rose diagrams (Figure 8b and c) which cover the three month period and a 15 month period, respectively. The first rose (Figure 8a), prepared using hourly data, is plotted at a smaller scale than the roses which were based on daily average wind velocity data (Figure 8b and c). Figure 8a and b covers the same time period and the much smaller amplitudes in Figure 8b reflect the depletion of high velocities due to averaging. Figure 8a and b both predict sand transport predominantly to the south during the three month study period. The year-round data contain a strong component of south winds, which are dominant during the rainy winter months; this is shown by the sand rose in Figure 8c as a significant component of sand transport to the north.

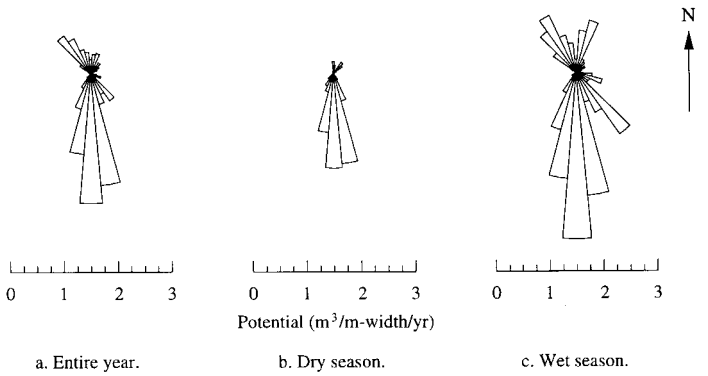

Figure 9. Sand transport potential based on wind data from PG&E, southern Humboldt Bay, 1965–67. (a) Annual data; (b) dry season; (c) wet season

Annual wind data collected by Pacific Gas and Electric (PG & E) at the Humboldt Bay Power Plant (located at the southern end of Humboldt Bay) in 1966/67 were used to prepare additional sand roses shown in Figure 9a–c. Although these data were recorded several years before the sand transport measurements in this study, they help to describe the general wind regime of the region. The PG & E data were recorded using an azimuthal bin size of 10° (vs 45° for the Eureka Weather Service data), and an anemometer height of 76 m (vs 27 m for the Eureka data). Sand transport is again underpredicted by the PG & E data, though not nearly as severely as in the case of the Eureka Weather Service data. The PG & E data were used to prepare the rose diagrams in Figure 9 for (a) annual, (b) dry season and (c) wet season data. As in the sand roses prepared from the Eureka Weather Service data (Figure 8a and b), the dry season data predict sand transport predominantly towards the south. The wet season data (Figure 9c) again predict a substantial reverse transport component.

Resultant transport direction

The vector sum of sand displacements predicted for individual azimuths gives the resultant displacement (Bagnold, 1941, p. 184–187; Fryberger and Dean, 1979). The resultant vector discharge may be written:

$$\mathbf{P}_{\text{res}} = \sum_{\theta} P_{\theta} \mathbf{e}_{\theta} \tag{11}$$

where $\mathbf{e}_{\theta}$ = unit vector of wind potential for azimuth θ.

The direction of the resultant sand transport $\mathbf{P}_{\text{res}}$ computed from the Eureka wind data was 169° (SSE). This is in excellent agreement with the 164° orientation of local wind-formed valleys and ridges, given the 45° bin size of the original wind data.

DISCUSSION

Field measurement of sand transport

The modelling approach used in this study assumes that slipface advance rates accurately reflect overall sand transport rates. The slipfaces monitored in this study spanned most of the widths of active corridors of sand, thus their migration rates should reflect typical transport rates in the corridors. Some transport also occurred in narrow longitudinal troughs along the lateral boundaries of the active zones, but this appeared to be of minor importance and was not monitored.

Slipface height was measured at the outset of the observation period, and changes in slipface height were assumed to be minor compared to horizontal advance rates. This assumption should be tested in future work by monitoring slipface height along with horizontal displacement.

Variations in wind due to site

Inconsistencies between theoretical and observed sand transport in this study were probably due to differences between wind velocities at the dunes and the Eureka Weather Service. Such differences could result from both natural causes and data acquisition technique. The dunes site is open and exposed to winds arriving from the Pacific Ocean, whereas the Eureka Weather Service is in downtown Eureka, nearly two miles from where the dominant NNW sand-driving winds first arrive onshore at the Samoa peninsula. Thus we expect wind velocities to be lower at the Eureka Weather Service than at the dunes, and similarly that sand transport estimates based on the Eureka wind data should be lower than transport rates observed at the dunes. The large difference between predicted and observed transport rates does not necessarily imply a large difference between wind velocities at the two sites; the transport model is highly sensitive to differences in wind velocity when maximum observed velocities are close to threshold velocity, as is the case in the present data set. For example, when observed wind velocities are multiplied by 1·6, predicted sand transport increases by a factor of ten and is in approximate agreement with observed transport.

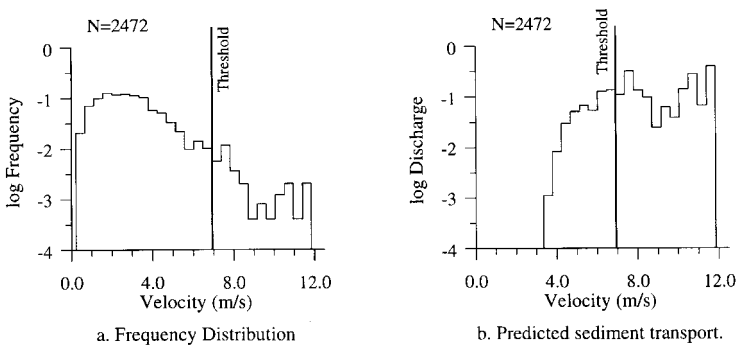

Figure 10. (a) Wind velocity versus frequency, hourly observations. (b) Transport potential. Only values to the right of the threshold velocity line contribute to the predicted transport

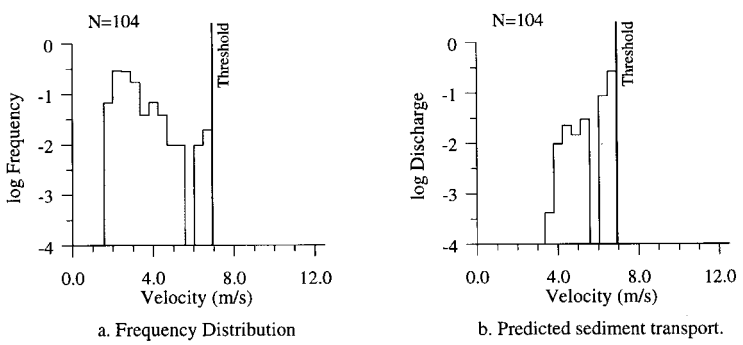

Figure 11. (a) Wind velocity versus frequency, daily observations. (b) Transport potential. No transport is predicted based on these data because threshold velocity is never exceeded

The sand transport model and wind data

Sand transport computed using field wind data with Bagnold-type transport models has been overpredicted in some studies (Hunter *et al.*, 1983; Goldsmith *et al.*, 1990) and underpredicted in others (Illenberger and Rust, 1988). Sarre (1988) found that the Bagnold equation overpredicted transport at low shear velocities but underpredicted it at higher shear velocities.

The Bagnold model does not account for the effects of vegetation, moisture and irregular topography, all of which tend to inhibit sand transport, Bauer *et al.* (1990) noted that such models were derived for equilibrium systems in which there are uniform flow conditions, and thus tend to overpredict transport rates in general field use.

In the present study, observed transport rates were underpredicted. This may be due to sampling effects. Wind velocity data from wind-tunnel experiments tend to be tightly controlled and well known, whereas weather bureau data are often only an averaged approximation of highly variable winds. It follows that empirical models derived from such laboratory experiments will underpredict sand transport when used with weather bureau wind data that have suffered depletion of high-velocity gusts due to averaging.

Frequency distribution of wind velocities

Discrepancies between theoretical and observed sand transport can be caused by the methods used to sample the wind data, both during and after data acquisition. The wind velocity data used in this study were originally collected in the form of hourly observations at the Eureka office of the National Weather Service. Each recorded velocity is obtained as a 1 min average, which has a tendency to eliminate high-velocity gusts. The National Weather Service also publishes monthly summaries in which *daily* average wind velocities are reported. The daily averages are produced by averaging the 24 hourly values from each day, which further reduces the high-velocity component of the data.

Histograms of wind velocity versus frequency and the corresponding transport potential can be used to determine which winds are responsible for the bulk of sand transport (Chapman, 1990; Borowka, 1990). They can also be used to illustrate the impact of averaging on the wind velocity distribution. Two versions of the wind data from the study period were compared using velocity–frequency histograms and the corresponding potential histograms. Wind observations were sorted by velocity and binned using a velocity increment of $44{\cdot}7$ cm s^{-1} (the precision of the original data was 1 mi h^{-1}). The first data set consisted of the original hourly observations. Wind velocity versus the logarithm of the frequency (normalized number of observations) is shown Figure 10a. Transport potential was computed independently for each velocity bin and is shown in Figure 10b. Only the values of the histogram to the right of the line indicating threshold velocity contribute to the total predicted discharge. The second data set was composed of daily averages and is again displayed in the form of velocity versus frequency (Figure 11a) and the corresponding transport potential (Figure 11b). Note that the velocity spectrum for the second data set has suffered depletion of all events above the threshold velocity, and no sand transport is predicted.

Seasonal variations in wind

During the three month study period, average sand discharge was $12{\cdot}5$ m^3 per m width per year at the $2{\cdot}5$ m high transverse ridge and $8{\cdot}8$ m^3 per m width per year at the 10 m high slipface. These rates are expected to be substantially higher than year-round averages, since they were measured during the season with maximum sand-driving potential.

As shown by the sand roses, the dominant sand transport potential was towards the south during the dry season, with a reverse component during the wet season. There was negligible precipitation (less than 3 cm) during the three month study period, and the effects of moisture were not considered in the wind potential computations. For year-round modelling, however, the effects of moisture appear to be more important.

The parabolic dune slipface was monitored on a less frequent basis for over a year and sand transport was invariably to the south, despite a large reverse potential during the winter months. In addition to the transport-inhibiting effects of moisture, this dune is sheltered on the southeast side by dense forest. Hunter *et al.* (1983),

whose study also considered coastal dunes in the Pacific northwest United States, noted likewise that the wet southerly winds move relatively little sand compared to the dry northerlies, despite their similar potential.

CONCLUSIONS

Relatively simple field measurements can be used to model dune slipfaces in three dimensions and compute the volume of sediment displaced over time. This technique may be used to monitor sinuous slipfaces where sediment transport rates are not constant across the width of the slipface. Transport predictions based on slipface advance provide a minimum estimate of true transport rate, with most of the error arising due to sand blown clear of the slipface during peak winds.

Sand transport estimates based on summary wind data from remote locations should be checked by monitoring sediment transport in the field, even if for only a short period of time. Such estimates are sensitive to wind data sampling and recording methods as well as differences between winds at the anemometer location and site of sand transport observations. There are fundamental differences between the wind data that have been used to develop most transport models and those available from weather bureaux. The former are often derived from wind-tunnel experiments where wind velocity is well known (usually by being held constant for extended periods), whereas weather bureaux data tend to provide averaged versions of highly variable winds, and often have sample intervals of 1 h or more. The process of averaging eliminates high-velocity winds. The Bagnold model and related models are sensitive to errors in wind velocity, especially for values close to the threshold velocity.

ACKNOWLEDGEMENTS

I thank the many friends and colleagues without whose support this project could not have been completed. The Friends of the Dunes and Faculties of the Geology and Geography Departments at Humboldt State University (HSU) provided encouragement and cooperation throughout the period of field work. Professor John Harper introduced me to the Lanphere Dunes, and he and David Gordon showed me the trails through the preserve. Dunes staff members Linda Miller and Kathie Kelly provided access to reports and air photos. HSU Professors Don Garlick and Bud Burke provided encouragement and critical review in the early stages of the work. Professor Garlick also deployed his balloon photography system, which provided excellent large-scale aerial images of the dunes. Dave Toronto and Orville Robinson of the National Weather Service in Eureka provided access to wind data. John St. Marie of the Friends of the Dunes provided the air photos that are shown in this paper. Bill Weaver of Pacific Watershed Associates provided a copy of his work on the dunes. Tom Ross of the National Climatic Data Center answered questions concerning wind data acquisition procedures. John Schaefer and Jim Ellis carefully read drafts and made many helpful suggestions. Discussions with Hugh Miller also led me to clarify some vague points. The anonymous reviewers are responsible for an improvement in both the technical presentation and general organization of this work.

REFERENCES

Anderson, R. S. 1988. 'The pattern of grainfall deposition in the lee of aeolian dunes', *Sedimentology*, **35**, 175–188.

Bagnold, R. A. 1941. The Physics of Blown Sand and Desert Dunes, Methuen, London, 265 pp (reprinted 1984, Chapman and Hall, London).

Bauer, B. O., Sherman, D. J., Nordstrom, D. F. and Gares, P. A. 1990. 'Aeolian transport measurement and prediction across a beach and dune at Castro-ville, California', in Nordstrom, K. F., Psuty, N. P. and Carter, R. W. G. (Eds), Coastal Dunes: Form and Process, John Wiley, 39–51.

Borówka, R. K. 1990. 'The Holocene development and present morphology of the Leba Dunes, Baltic coast of Poland', in Nordstrom, K. F., Psuty, N. P., and Carter, R. W. G. (Eds), Coastal Dunes: Form and Process, John Wiley, 289–313.

Chapman, D. M. 1990. 'Aeolian sand transport–an optimized model', *Earth Surface Processes and Landforms*, **15**, 751–760.

Cooper, W. S. 1967. Coastal Dunes of California, Geological Society of America, Memoir **104**.

Fryberger, S. G. and Dean, G. 1979. 'Dune forms and wind regime', in McKee, E. D. (Ed.), A Study of Global Sand Seas, USGS Professional Paper 1052, 137–185.

Goldsmith, V., Rosen, P. and Gertner, Y. 1990. 'Eolian transport measurements, winds, and comparison with theoretical transport in Israeli coastal dunes', in Nordstrom, K. F., Psuty, N. P. and Carter, R. W. G. (Eds), Coastal Dunes: Form and Process, John Wiley, 79–101.

Hunter, R. E., Richmond, B. M. and Alpha, T. R. 1983. 'Storm-controlled oblique dunes of the Oregon coast', *GSA Bulletin*, **94**, 1450–1465.
Illenberger, W. K. and Rust, I. 1988. 'A sand budget for the Alexandria coastal dunefield, South Africa', *Sedimentology*, **35**, 513–521.
Johnson, J. W. 1963a. An ecological study of the dune flora of the north spit of Humboldt Bay, MS thesis, Humboldt State University.
Johnson, J. W. 1963b. Sand movement on coastal dunes, Institute of Engineering Technical Report **HEL-2–3**, University of California, Berkeley, 18 pp.
Lettau, H. H. and Lettau, K. 1978. 'Experimental and micrometerological field studies of dune migration', in Lettau, H. H. and Lettau, K. (Eds), Exploring the World's Driest Climate, University of Wisconsin-Madison, 110–131.
Livingstone, I. 1989. 'Monitoring surface change on a Namib linear dune', *Earth Surface Processes and Landforms*, **14**, 317–332.
McEwan, I. K. and Willetts, B. B. 1994. 'On the prediction of bed-load sand transport rate in air', *Sedimentology*, **41**, 1241–1251.
Mulligan, K. R. 1988. 'Velocity profiles measured on the windward slope of a transverse dune', *Earth Surface Processes and Landforms*, **13**, 575–582.
Pickard, J. 1972. 'Rate of movement of transgressive sand dunes at Cronulla, New South Wales', *Journal of the Geological Society of Australia*, **19** (2), 213–216.
Prandtl, L. 1934. 'The mechanics of viscous fluids', in Durand, W. F. (Ed.), Aerodynamic Theory, A General Review of Progress under a Grant of the Guggenheim Fund for the Promotion of Aeronautics, Vol. III, Julius Springer, Berlin, 34–208.
Sarre, R. D. 1988. 'Evaluation of aeolian sand transport equations using intertidal zone measurements, Saunton Sands, England', *Sedimentology*, **35**, 671–679.
Sarre, R. D. 1989. 'Aeolian sand drift from the intertidal zone on a temperate beach: potential and actual rates', *Earth Surface Processes and Landforms*, **14**, 247–258.
Weaver, W. 1991. Options for the Coastal Sand Dunes of Hurnboldt Bay, Humboldt County, California, prepared for Humboldt County Planning Department, Eureka, Ca., by Pacific Watershed Association.

